Plasma Shape Effects on Sawtooth / Internal Kink Stability and Plasma Shaping Using EC Wave Current Profile Tailoring in TCV

A. Pochelon, F. Hofmann, H. Reimerdes, C. Angioni, R. Behn, R. Duquerroy, I. Furno, T.P. Goodman, P. Gomez, M.A. Henderson, An. Martynov, P. Nikkola, O. Sauter, A. Sushkov*

Centre de Recherches en Physique des Plasmas, Ecole Polytechnique Fédérale de Lausanne, Association EURATOM-Confédération Suisse, CH-1015 Lausanne EPFL, Switzerland
* RRC, Kurchatov, Russia
e-mail contact of main author: Antoine.Pochelon@epfl.ch

Abstract. This paper addresses the effect of plasma shaping (triangularity and elongation) on the sawtooth stability as well as the technique of current profile broadening using off-axis electron cyclotron heating (ECH) to enlarge the stable operational range towards higher elongations. The plasma shape strongly influences the sawtooth period and amplitude. This effect is emphasised by ECH, with the sawtooth period becoming shorter at low triangularity or at high elongation; for these plasma shapes, the pressure profile inside q=1 remains essentially flat. A comparison of the sawtooth response with marginal Mercier stability shows that the critical pressure gradient at q=1 is particularly low for plasma shapes where the increased sawtooth repetition frequency prevents the peaking of the pressure profiles. For theses shapes, the ideal internal kink is also found unstable from stability calculations. The stability of highly elongated plasmas depends largely on current profiles. The operational range at low current has been extended towards higher elongation using ECH heated discharges. Far off-axis second harmonic X-mode ECH power deposition proves to be an efficient tool for current profile tailoring allowing a significant elongation increase at constant quadrupole field.

1. Introduction

The TCV tokamak (R=0.88 m, a=0.25 m, $I_p \leq 1$ MA, B<1.54 T, $\kappa<2.8$, $-0.7<\delta<0.9$) is particularly suited for the study of shape related issues. It is presently equipped with a total of 3 MW ECRH/ECCD power at the second harmonic, 82.7 GHz, injected by 6 independent launchers, steerable during the discharge, which allows for highly localised power deposition schemes [1].

2. Dependence of sawtooth / Internal kink stability on plasma shape

2.1 Triangularity and elongation effects with central ECH

In the TCV tokamak the sawtooth period and the sawtooth amplitude are observed to depend strongly on the shape of the poloidal plasma cross-section. Systematic scans of plasma elongation and triangularity ($0<\delta<0.5$, $1.2<\kappa<2.1$) show small sawteeth with short periods at high elongation or at low and negative triangularity, and large sawteeth with long periods at low elongation or high triangularity. Additional central electron cyclotron heating power further amplifies the shape dependence of the sawtooth properties. The sawtooth period can either increase or decrease with additional heating power depending on the plasma shape. As an example, FIG. 1 shows the increase of the sawtooth period with power deposited inside the q=1 surface at high triangularity and the decrease at low triangularity. Similarly, the sawtooth period decreases for high elongations [2].

An analytic expansion of the Mercier criterion [3] suggests that low triangularity and high elongation lead to a lower ideal MHD central pressure limit, as shown in FIG. 2 for the shape parameters of the q=1 surface. These analytic results are confirmed by ideal MHD calculations using the KINX code [4], which show that the internal kink mode is unstable for the lowest triangularity and highest elongation cases of FIG. 2, and stable for the highest triangularity and lowest elongation cases. Therefore, for plasma shapes where additional heating and, consequently, increased central pressure gradients shorten the sawtooth period, the low central pressure gradient limit achieved is consistent with ideal MHD predictions of internal kink stability. This is expressed by a limitation of the poloidal beta on the q=1 surface (see e.g. [2]): $\beta_{p,1}=(\langle p\rangle_1-p(\rho_1))/(B_p^2(\rho_1)/2\mu_0)$, where the numerator represents the volume averaged

incremental pressure above the pressure at q=1. In addition, the experimentally observed sawtooth behaviour is consistent with a sawtooth trigger model, which assumes the ideal or resistive internal kink to be responsible for the sawtooth crash [5]. The results of FIG. 1 exhibit two triangularity ranges: for $\delta \leq 0.2$, where the sawtooth period decreases with power in accordance with the destabilising effect of central pressure on internal kink stability; and for $\delta \geq 0.3$, for which the increased pressure gradients are stabilising through increased ω_e* [5].

Ideal KINX code results also show the internal kink stability to be dependent on shape parameters [6]. The ideal internal kink is shown to be unstable at triangularities in the range $-0.14<\delta_1<0.11$ for elongations typically $\kappa_1>1.3$, this elongation limit decreasing slightly with $\beta_{p,1}$. At higher or lower δ_1, the mode becomes stable. The domain over which τ_{ST} was investigated in TCV is within this triangularity range. In the experiment, discharges with elongation $\kappa_1>1.3$ show indeed a shortening of τ_{ST} with P_{EC} (see FIG. 2).

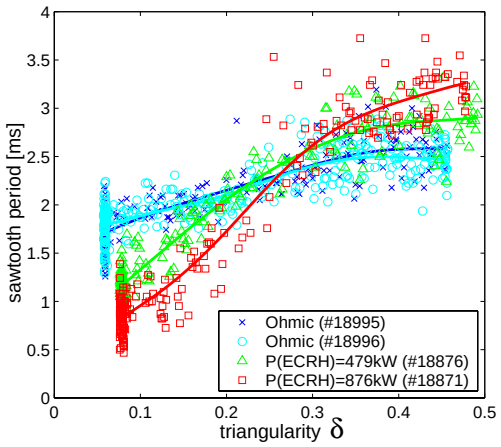

FIG. 1 Sawtooth period as a function of triangularity δ for an ohmic discharge with κ~1.5 and different ECRH powers injected inside q=1. The sawtooth period decreases for low triangularity, δ<0.2-0.3 and increases above. Electron density and sawtooth inversion radius were kept constant (ρ_{inv}~0.5, $q_{eng}=5abB/RI_p$~2).

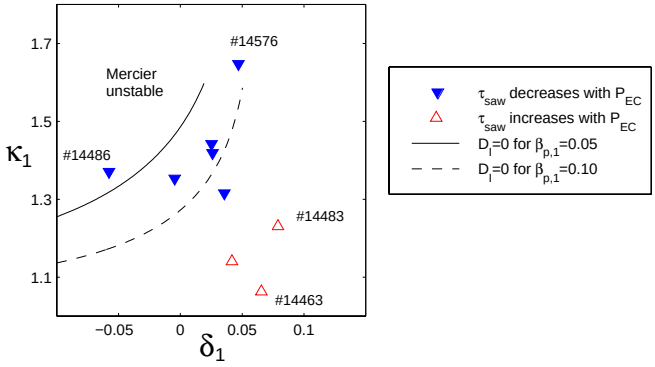

FIG. 2 The discharges of different shapes are shown as a function of triangularity and elongation of the q=1 surface. The plasma shapes are compared to the shapes corresponding to marginal stability according to the Mercier criterion [3] for two different values of $\beta_{p,1}$ and assuming constant shear $s_1=\rho_1(dq/d\rho_1)=0.1$ and inversion radius $\rho_{inv}=0.5$.

Direct measurements of the n=1 exponential growth rate γ from magnetic and/or soft X-ray signals have also been attempted, e.g. in JET [7] and TCV. In TCV, this γ increases with triangularity ($0<\delta<0.5$), and appears to be in contradiction with the Mercier stability and the sawtooth period data [2]. The measured γ scales with the amplitude of the crash pressure drop, which increases with the longer sawteeth at high triangularity. However, the experimental γ can only be measured in the late non-linear phase of the crash, and is not necessarily related to the linear γ, which probably remains below noise level.

2.2 Extreme elongation ohmic behaviour ($2.3<\kappa<2.8$)

Extremely elongated ($2.3<\kappa<2.8$) ohmic plasmas have been created in TCV at low q. In these discharges, the sawtooth period, τ_{ST}, decreases with elongation, FIG. 3, extending earlier results [2, 8] to even higher elongation. The sawtooth period is normalised to the density, which folds ramp-up and ramp-down values together. Therefore, the τ_{ST} values are not the result of transients. This normalisation is justified by the proportionality $\tau_{ST} \sim n_e$ found in several tokamaks [9, 10] and confirmed in TCV for different elongations (κ=1.6, 2.2), at similar measured inversion radii (ρ_{inv}~0.40-0.45) for densities ranging from 2 to 5 10^{19}m^{-3}.

When the elongation is increased, see FIG. 3, a first discontinuity is seen at κ~1.9, after which the sawtooth period and relative fluctuation amplitude continue to decrease up to an elongation κ~2.3-2.6, where the sawteeth abruptly disappear below resolution. This abrupt transition occurs at a very precise value of the internal inductance, l_i~0.69 (at low q, large ρ_1), see FIG. 4. The sawtooth inversion radius, ρ_{inv}, remains approximately constant. It does not vary significantly prior to the transition (typically ~ 0.49±0.03), and may vary somewhat more after the transition, where some small randomly re-occurring sawteeth allow its determination, even below l_i~0.69. The electron temperature profile remains practically unchanged through the transition. Therefore, with or without sawteeth, it is very flat in the centre and shows a sharp rollover in the ρ_{inv} region, suggesting that ρ_1 does not change during this transition.

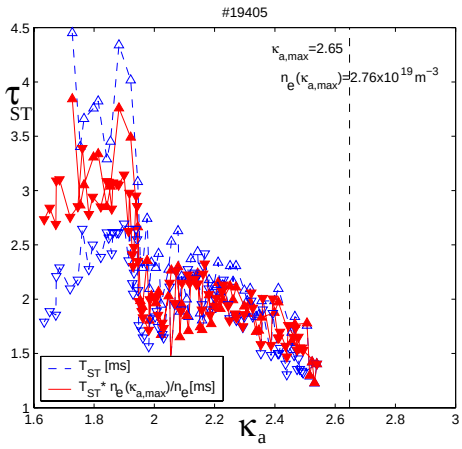

FIG. 3 Decrease of the sawtooth period τ_{ST} with elongation and sawtooth disappearance at κ~2.5. The normalisation to n_e (full triangles) cancels the ramp-up/-down hysteresis.

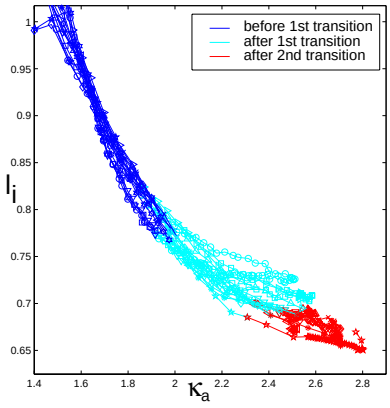

FIG. 4 Abrupt disappearance of sawteeth below an internal inductance of l_i=0.69 for different n_e and dI_p/dt.

Higher toroidal modes, n=2, 3, 4, measured with magnetic probes, are observed at high elongation. Thus, there are several indications supporting the existence of unstable modes at extreme elongation which flatten the core temperature profile even though the macroscopic sawteeth have disappeared.

2.3 Conclusion

In these experiments, the observed sawtooth period has been successfully used to link the experiment with the Mercier ideal stability criterion and with internal kink stability. The flexibility in plasma shape of TCV has therefore allowed: 1) the experimental determination of the effect of plasma shape and central pressure on sawtooth stability, 2) the demonstration of the contribution of the ideal internal kink mode in triggering the sawtooth crash at high elongation and at low triangularity [2].

3. Current profile modifications to increase plasma elongation

The stability of highly elongated plasmas depends largely on current profiles [11]. At high elongation, low current high q discharges are unstable with respect to axisymmetric modes. We present initial experiments using EC wave current profile broadening to create and stabilise high elongation, low current discharges, which would be ohmically unstable, thus reducing the strong correlation between κ and l_i in ohmic plasmas at fixed current (FIG. 4).

Among the different EC-schemes, the current profile can be broadened by off-axis ECH, on axis counter-ECCD or off-axis co-ECCD. PRETOR transport code simulations [12, 13] using the local RLW heat transfer coefficients [14] favour off-axis ECH. Let us consider the requirements for maximising the current density in the outer half of the profile. In general, simulations show that the current density j(ρ) is increased above ohmic at the deposition radius, ρ_{dep}, and in a layer of finite thickness outside of it. Hence, the optimal ρ_{dep} to increase j(ρ~0.7)

is typically ρ_{dep}~0.7. Moving ρ_{dep} too far in, typically ρ_{dep}<0.5, is seen to decrease j(ρ~0.7). The experimental task is then the determination of an optimum deposition location in the outer half of the profile, which maximises both elongation and plasma stability. Central counter-ECCD increases the current in a ring inside ρ~0.65 and decreases it further out, making it less attractive than off-axis ECH, which was also confirmed experimentally.

The standard EC set-up uses 2-4 gyrotrons, a maximum of 2MW shared between upper lateral and equatorial launchers, in off-axis ECH. The discharges are pre-programmed for a constant quadrupole field throughout the ohmic and EC heated phases. Using a high pre-programmed triangularity, similar to that used in ohmic discharges, led to 8% indentation in the mid-plane on the HFS in the EC phase, a wider gap on the LFS and very high central elongation k_0~k_{edge}. By decreasing the triangularity, the indentation was removed and the elongation on axis reduced, which improves stability and spreads the power more uniformly onto the tiles. This allowed operation at high elongation and low current (κ=2.4, q=13, I_p=300kA, $\langle j \rangle/(q_0 j_0)$~0.22), which would not have been possible with peaked ohmic profiles. As a comparison, ohmic discharges at elongation κ=2.4 were typically obtained at current densities which were higher by a factor 2.5.

With an injection of 1.9MW using 4 static EC beams at ρ=0.65 initially, the initial ohmic elongation of 1.75 increases to 2.40 in 0.37s, while the deposition gradually moves to smaller radii, ρ=0.5. Meanwhile, the internal inductance l_i decreases from 1.25 to 0.83, which can be attributed to both the increased elongation and the flattened current profile. Growth rates of the vertical instability, as obtained from a rigid displacement model [15] are γ_R=996s^{-1} in the ohmic phase and γ_R=2688s^{-1} just before the disruption. The latter value corresponds to a very low stability margin and, consequently, we are close to the maximum elongation at I_p=300kA.

The discharge stability was improved by reducing the injected power to 1MW and moving the ECH deposition out during the elongation process. This allowed completely stable non-disruptive discharges at κ=2.4, FIG. 5, with γ_R=2238s^{-1} at the highest elongation, t=1.4s. The lower beam is moved out (FIG. 5b) during the discharge to keep the deposition location

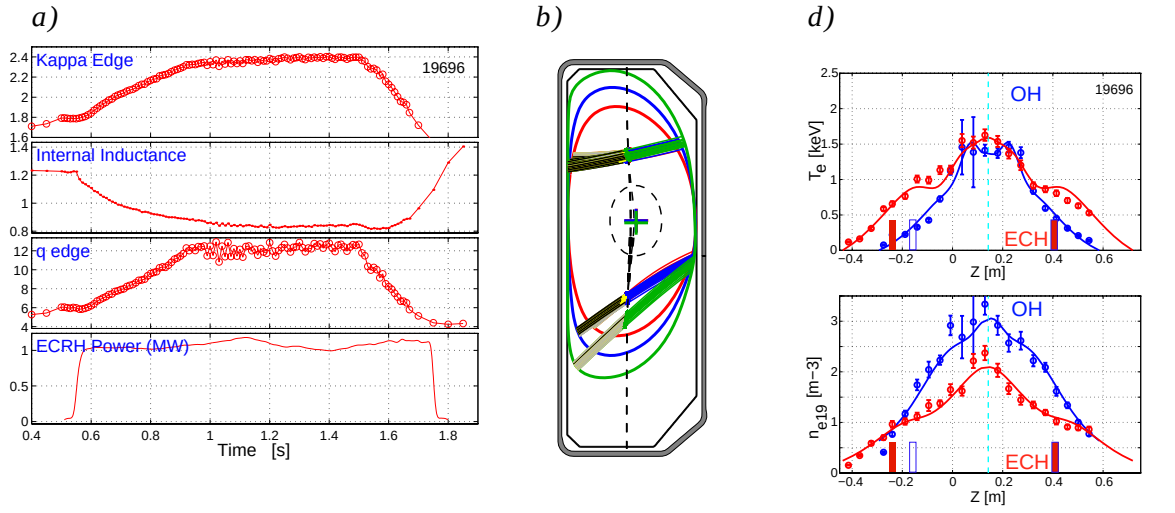

FIG. 5. Low current high elongation made possible by off-axis ECRH current profile broadening. a) Elongation grows from 1.8 to 2.4 with 1MW ECRH. b) Poloidal view with plasma shape and beams at three times (t=0.55, 0.75, 1.4s), cold resonance and q=1 surface at initial ohmic time. c) Deposition in the outer half of the profile, with lower launcher moving out during the shot. c) Thomson T_e and n_e profile in ohmic phase (blue) and at highest κ during ECRH (red, t=1.4s).

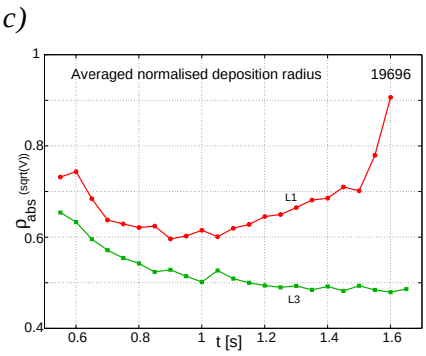

approximately constant at ρ_{dep}~0.7 (FIG. 5c), which allows a more economical use of the deposited power while elongating. The ECH power was shut off only after the pre-programmed elongation ramp-down, permitting a soft termination of the discharge. The electron temperature profile is broadened, with a distinct shoulder at the power deposition location, see FIG. 5d top. The density profile is strongly modified with a pump-out effect removing density from the deposition location, pushing it to the centre and to the edge. This explains strong density peaking on axis and a high gas injection rate to compensate for the outward flux. A power balance analysis shows that the heat flux and the electron conductivity χ_e is strongly reduced to values below the ohmic level inside the deposition radius and increased outside.

Soon after the heating starts, the central q_0 moves above unity and sawteeth disappear. Due to the ρ_{dep} sweep during the discharge and the induced q-profile change, the power deposition location crosses integer-q surfaces. However no deleterious MHD was noticed in these high q discharges. The final elongation depends only weakly on power. It also depends weakly on the location of the power deposition as long as the deposition occurs in the outer half of the profile.

However, there is an outer limit for the initial deposition radius beyond which the first-pass absorption is too low to embark on an elongation process. A successful elongation run was still obtained with 2MW and starting the deposition as far out as ρ~0.8, with a first-pass absorption below 50% (n_{e19}~0.7, T_e~0.3keV at the absorption layer). Lowering the power to 1MW required a more central initial deposition location.

3.1. Conclusion

Far off-axis second harmonic X-mode ECH power deposition proves to be an efficient tool for current profile tailoring allowing a significant elongation increase at fixed quadrupole field. The operation at low current and high elongation has been substantially extended with off-axis ECH current profile broadening, making low current operation possible at current densities 2.5 times lower than in similar ohmic plasmas. From the present experience, stable high elongation discharges at κ>2.4 will require higher currents, since the axisymmetric growth rate is close to the limit. Furthermore, the exploitation of the high β potential of elongated discharges would require a normalised current around I_N=I/aB~2.0MA/mT, a factor of 2 above the 0.84MA/mT achieved here. This opens a new area for confinement and stability limit studies at high elongation, e.g. combining X2 current profile broadening and X3 central heating [16].

Acknowledgement: This work was partly supported by the Swiss National Science Foundation.

References:

[1] GOODMAN T.P. et al., 19th Symp. on Fusion Technology, Lisbon, Portugal, 1996.
[2] REIMERDES H., POCHELON A., SAUTER O., GOODMAN T.P., HENDERSON M.A., MARTYNOV An.A., Plasma Phys. Contr. Fusion **42** (2000) 629.
[3] LÜTJENS H., BONDESON A. and VLAD G., Nucl. Fusion **32** (1992) 1625.
[4] DEGTYAREV L., MARTYNOV A., MEDVEDEV S., TROYON F., VILLARD L., GRUBER R., Comput. Phys. Commun. 103 (1997) 10.
[5] PORCELLI F., BOUCHER D. and ROSENBLUTH M.N., Plasma Phys. Contr. Fus. **38** (1996) 2163.
[6] MARTYNOV An. and SAUTER O., Proc. of Theory of Fusion Plasmas, Varenna 2000, (Editrice Compositori, Bologna, 2000), (to be published).
[7] DUPERREX P.A., POCHELON A. et al., Nucl. Fusion **32** (1992) 1161.
[8] POCHELON A., GOODMAN T.P., HENDERSON M.A. et al., Nucl. Fus. **39**, No.11Y (1999) 1807.
[9] TFR-Group, Proc. 6th Int. Conf. on Plasma Phys. and Contr. Nucl. Fus. Research, Berchtesgaden Vol. I (1976) 279.
[10] SIMM W., Thesis, Lausanne Laboratory Report LRP 334/87 (1987).
[11] HOFMANN F. et al., Phys. Rev. Lett. **81**, 2918 (1998).
[12] ANGIONI C. et al., ibid., (to be published).
[13] BOUCHER D. and REBUT P.H., in Proc. IAEA Tech. Com. on Advances in Simulation and Model. of Thermonuclear Plasmas, 1992, Montreal (1993) 142.
[14] REBUT P.H., LALLIA P.P. and WATKINS M.L., Proc. 12th Int. Conf. Plasma Physics and Controlled Nuclear Fusion Research, Nice 1988, IAEA Vienna 1989, Vol. 2, 191.
[15] HOFMANN F. et al. Nuclear Fusion **38** (1998) 1767.
[16] ALBERTI. S. et al., Proc. 18th IAEA Fusion Energy Conf. paper PD/2.